Acta Oceanol. Sin., 2021, Vol. 40, No. 11, P. 138–146
https://doi.org/10.1007/s13131-021-1832-0
http://www.aosocean.com
E-mail: ocean2@hyxb.org.cn

Geological characteristics of the Qiaoyue Seamount and associated ultramafic-hosted seafloor hydrothermal system (~52.1°E, Southwest Indian Ridge)

Yongjin Huang[1, 2], Chunhui Tao[1, 2, 3*], Jin Liang[1, 2*], Shili Liao[1, 2], Yuan Wang[1, 2], Dong Chen[4], Weifang Yang[1, 2]

[1] Key Laboratory of Submarine Geosciences, Ministry of Natural Resources, Hangzhou 310012, China

[2] Second Institute of Oceanography, Ministry of Natural Resources, Hangzhou 310012, China

[3] School of Oceanography, Shanghai Jiao Tong University, Shanghai 200030, China

[4] College of Oceanography, Hohai University, Nanjing 210098, China

Received 3 January 2021; accepted 26 March 2021

Abstract

Hydrothermal vent incidence was once thought to be proportional to the spreading rate of the mid-ocean ridges (MORs). However, more and more studies have shown that the ultraslow-spreading ridges (e.g., Southwest Indian Ridge (SWIR)) have a relatively higher incidence of hydrothermal venting fields. The Qiaoyue Seamount (52.1°E) is located at the southern side of segment #25 of the SWIR, to the west of the Gallieni transform fault. The Chinese Dayang cruises conducted eight preliminary deep-towed surveys of hydrothermal activity in the area during 2009 and 2018. Here, through comprehensive analyses of the video and photos obtained by the deep-towed platforms, rock samples, and water column turbidity anomalies, a high-temperature, ultramafic-hosted hydrothermal system is predicted on the northern flank of the Qiaoyue Seamount. We propose that this hydrothermal system is most likely to be driven by gabboric intrusions. Efficient hydrothermal circulation channels appear against a backdrop of high rock permeability related to the detachment fault.

Key words: Southwest Indian Ridge, Qiaoyue Seamount, hydrothermal activity, detachment fault

Citation: Huang Yongjin, Tao Chunhui, Liang Jin, Liao Shili, Wang Yuan, Chen Dong, Yang Weifang. 2021. Geological characteristics of the Qiaoyue Seamount and associated ultramafic-hosted seafloor hydrothermal system (~52.1°E, Southwest Indian Ridge). Acta Oceanologica Sinica, 40(11): 138–146, doi: 10.1007/s13131-021-1832-0

1 Introduction

Seafloor hydrothermal activity is an important way of material and energy circulation between the ocean and solid earth (Hasenclever et al., 2014), which manifests in different seafloor tectonic environments, such as ocean spreading ridges and arc volcanoes (Baker and German, 2004; Beaulieu et al., 2015; Baker et al., 2016). Approximate 65% of hydrothermal vent fields are distributed on the mid-ocean ridges (MORs) (Hannington et al., 2011). Since the first seafloor hydrothermal vent was observed at the Galápagos Rift in 1977 (Corliss et al., 1979), hydrothermal activity has attracted considerable interest. To date, approximately 500 confirmed and inferred submarine hydrothermal fields have been reported on the MORs (data source: http://vents-data.interridge.org/), of which ~60 have been reported on ultraslow-spreading ridges (full spreading rate: <20 mm/a) (Beaulieu et al., 2013). German et al. (1995) suggested that hydrothermal activity on slow and ultraslow-spreading ridges was restricted because of a lower melt supply. Furthermore, Baker et al. (1996) proposed that hydrothermal vent incidence was proportional to the spreading rate of the MORs. However, a relatively higher frequency of hydrothermal activity on the ultraslow-spreading Southwest Indian Ridge (SWIR) was demonstrated (German et al., 1998), and large-scale seafloor massive sulfide deposits were suggested to be more likely to form along the ultraslow-spreading ridges (German et al., 2016). As per the empirical relationship between the incidence of hydrothermal plumes and spreading rate, Beaulieu et al. (2015) predicted that there are ~130 active hydrothermal venting fields yet to be discovered on the ultraslow-spreading ridges.

Tracking of hydrothermal plume, which is formed by the mixing of hot vent fluids and ambient seawater, is a potent method for locating and characterizing seafloor hydrothermal discharges (Tao et al., 2017). Turbidity measurements are by far the commonly used tool for hydrothermal surveys (Baker et al., 2004, 2016; Tao et al., 2017). There is a strong relationship between the intensity of water turbidity anomalies and distance from active high-temperature vent sites. For example, the value of turbidity anomalies nearby the vent with fluid temperature of 350°C can reach 0.4 ΔNTU (Nephelometric Turbidity Units) (Chen et al., 2014), and the value detected 3.5 km away from high-temperature Zouyu-2 hydrothermal field on the Mid-Atlantic Ridge is ~0.02 ΔNTU (Tao et al., 2017). By contrast, low-temperature and

Foundation item: The National Key Research and Development Program of China under contract No. 2016YFC0304905; the National Natural Science Foundation of China under contract No. 41806076; the Scientific Research Fund of the Second Institute of Oceanography, MNR under contract No. JG1804; the China Ocean Mineral Resources R&D Association (COMRA) Major Project under contract Nos DY135-S1-1-01, DY135-S1-1-02 and DY135-S1-1-09.

*Corresponding author, E-mail: taochunhuimail@163.com; kamleung@aliyun.com

diffused venting usually show little or no turbidity anomalies (Chen et al., 2019; Li et al., 2020).

The investigation of hydrothermal activity along the SWIR has predominantly focused on segments #27 and #28 which identifies the Longqi, Duanqiao, and Yuhuang hydrothermal fields (Han et al., 2010; Tao et al., 2012; Yang et al., 2017). Furthermore, the Tiancheng and Tianzuo hydrothermal fields were discovered in the eastern SWIR in 2009 (Tao et al., 2009; Chen et al., 2018). However, the investigations of other segments of the SWIR are relatively limited. During 2009 and 2018, the Chinese Dayang cruises conducted eight deep-towed surveys at the Qiaoyue Seamount, with lines of ~120 km in length and ~4 km apart to identify signals of hydrothermal activity. In this study, through analyzing water column turbidity anomalies and hydrothermally affected debris, we predict that a high-temperature hydrothermal field in ultramafic rocks exists at the footwall of the detachment fault on the northern flank of the Qiaoyue Seamount. In addition, we depict a generalized regional geological map of the seamount based on observations from video and photos, and rock sampling, in order to better understanding the geological characteristics of the study area. Finally, we present an overview of the distinct tectonic setting of Qiaoyue Seamount and describe the local geologic controls on the vent field.

2 Geological setting

The SWIR has a total length of ~8 000 km, extending from the Rodrigues Triple Junction (RTJ) to the Bouvet Triple Junction (BTJ), and is classified as an ultraslow-spreading ridge with a full spreading rate of ~14 mm/a (Muller et al., 1999). Extremely thin or missing crust and extensive exposure of mantle-derived material are reported along the SWIR (Dick et al., 2003; Zhou and Dick, 2013). The average thickness of the oceanic crust along the SWIR is 4 km (Cannat et al., 2008), which is much thinner than the global average of ~7 km (Baker and German, 2004). However, the oceanic crustal thickness at SWIR 50°28′E is up to 9.5 km, demonstrating the presence of an extreme magmatic accretion beneath the region (Li et al., 2015; Jian et al., 2017). Three types of seafloor geomorphology are observed in the SWIR: volcanic seafloor (volcanic cones and flat-topped volcanoes), smooth seafloor, and corrugated seafloor (Cannat et al., 1999, 2006). The rocks exposed on the seafloor are mainly composed of basalts, with some gabbros and serpentinized peridotites, which feature local outcrops adjacent to the fracture zones and detachment faults (Dick et al., 2000; Tao et al., 2011).

The SWIR is characterized by extremely rugged topography and an axial rift valley with water depths of $<$–5 000 m, and is offset by a series of north-south striking transform faults (Georgen et al., 2001). Owing to the Marion and Crozet hotspots to the southwest of the SWIR, the ridge segment between the Indomed and Gallieni transform faults (46°–52.3°E) shows strong negative residual mantle Bouguer gravity anomalies, indicating a relatively active crust–mantle exchange and deep magmatism in this region, as well as moderate levels of melt and heat supply (Georgen et al., 2001; Sauter et al., 2001, 2009; Cannat et al., 2008).

The Qiaoyue Seamount, located on the southern side of segment #25, is close to the Gallieni transform fault (Fig. 1). This ridge segment shows asymmetric spreading features. Moreover, the east-northeast striking segment is about 29 km long with an average oceanic crustal thickness of ~1.8 km, an effective spreading rate of 12.63 mm/a, and an average axial water depth of –4 751 m (Liu, 2019). The *M* factor (the fraction of the total plate separation taken up by the accretion of melt) (Buck et al., 2005) of segment #25 calculated by Liu (2019) (i.e., segment #13 in his study) is ~0.3, which indicates a relatively lower magma supply. The Qiaoyue Seamount is situated ~12 km away from the ridge axis with a water depth ranging from –1 400 m to –4 200 m. The terrain of the northern side of the seamount is corrugated, whereas the southern side exhibits a relatively rugged seafloor. Previous sampling surveys indicate that rocks exposed on the seafloor in the study area are primarily peridotites and serpentinized peridotites (Supplementary Table S1), although basaltic and/or volcanic debris have been sampled in certain areas.

3 Data and methods

Data presented here were acquired during two cruises on the Qiaoyue Seamount (Table 1). During the 20VII leg in 2009 and 49IV leg in 2018, plume surveys were conducted in the study area using a deep-towed instrument package equipped with RBR turbidity sensors, manufactured by the Canadian RBR company, and underwater high-definition cameras. The position of deep-towed instrument package relative to the ship, which was located using the differential global positioning system, determined by ultra-short baseline positioning system. A series of RBRs were connected at set intervals along a cable, forming a ~300 m vertical RBR array to detect hydrothermal plume signatures.

Turbidity measurement by RBR was based on the principle of backscatter. The light emitted by the sensor was scattered back to the sensor by the suspended particles in hydrothermal plume. The received light intensity was transformed into a voltage reading, which was then converted to seawater turbidity in terms of NTU, based on the laboratory calibration using formazine. ΔNTU was the plume optical anomaly in excess of the ΔNTU value of local ambient deep waters (Baker and German, 2004). A series of processing steps were applied to the turbidity data, including correction for position deviation, data de-noising, and systematic error correction (Chen, 2016). The data were collected from eight deep-towed survey lines (Fig. 2a) and the 49IV-L003SHX02 (i.e., line ③ in Fig. 2a) line is worth noting.

Additional data in our study area were a large amount of video and photos recorded by underwater cameras. This provided us a unique opportunity to draw a generalized regional geological map of the Qiaoyue Seamount, which can help to better understand the geological characteristics of the seamount. We distinguished the substrate type (Fig. 2a) through analyzing video and photos of each survey line. Each survey line then could be divided into a lot of points, corresponding to their substrate attribute. Nearby points with the same substrate attribute on two adjacent survey lines would be artificially expanded into the surface as a substrate unit. The boundary of different substrate units was usually set in the middle of adjacent survey lines and depicted by the dotted line. Then, the sampling results are used to verify the substrate type determined by images. The boundary of individual samplings was extrapolated of ~1 km, represented by the solid lines. The above work was conducted by ArcGIS software. Finally, we deciphered and draughted a generalized geological map of the Qiaoyue Seamount, which covered ~600 km^2 (Fig. 2a).

4 Results

4.1 *Regional geological mapping*

The study area was mostly covered by pelagic sediments, which is more likely to deposit in depressions and flat crests on the seamount (Fig. 2). The types of sediment are dominantly controlled by the carbonate compensation depth (CCD). The water depth of the Qiaoyue Seamount is shallower than the CCD of –4 800 m in the 30°~40°S area of the Indian Ocean (Kolla et al.,

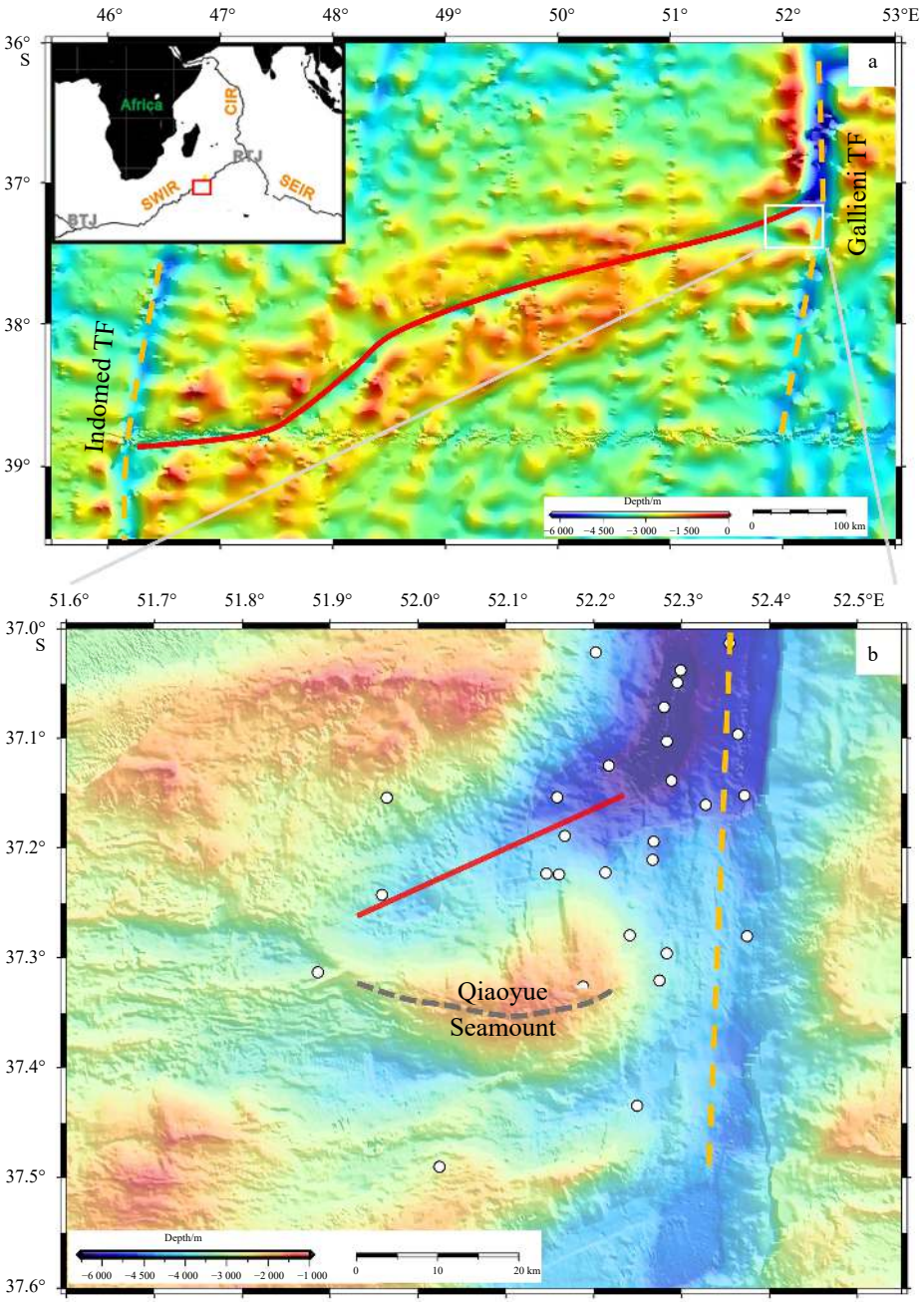

Fig. 1. Bathymetric map of the Southwest Indian Ridge between the Indomed transform fault (TF) and Gallieni transform fault (TF), with the location of the Qiaoyue Seamount (a) and high-resolution bathymetric map of the Qiaoyue Seamount on the SWIR (b). Inset shows the location of Fig.1a in the SWIR. The bathymetric data were collected by multi-beam surveys. The red solid line in Fig.1a shows the first-order ridge axis between the Indomed TF and Gallieni TF. The white dots in Fig.1b show the epicenter of the study area (data source: http://www.isc.ac.uk/). The red solid line in Fig.1b indicates the axis of segment #25 (second-order ridge). The gray dotted line in Fig.1b shows the upper limit of a large fault. The second-order segments cited in the text and/or other figures are identified by their numbers, following the nomenclature of Cannat et al. (1999) and Liu (2019). BTJ: Bouvet Triple Junction; RTJ: Rodrigues Triple Junction; CIR: Central Indian Ridge; SEIR: Southeast Indian Ridge.

1976). Therefore, the sediments are predominantly gray-white calcareous oozes with a low content of pelagic clays and lithogenic detritus, and they are primarily derived from the calcareous shell remains of foraminifera, which has been confirmed by samplings. Furthermore, ripple marks are visible on certain of the surface sediments in the study area (Fig. 2b), indicating the effects of strong bottom currents. Given its shape and the direction of camera movement, we propose that the primary direction of bottom current along the two flanks of the Qiaoyue Seamount is east-to-west in our study area, possibly owing to partial deflection of the south-to-north Antarctic bottom stream (McCave et al., 2005) when flowing into the Qiaoyue Seamount along the Gallieni transform fault.

The ultramafic and/or mafic breccia/debris are primarily distributed on the seamount crest and assumed to be modified by normal/detachment faults. Relatively concentrated pillow lava is

Table 1. Cruise chronology on the Qiaoyue Seamount

Cruise and leg	Ship	Line No.	Date
The 7th leg of Chinese 20th Cruise (20 VII)	*Dayang Yihao*	20VII-L6SHX5	Feb. 5, 2009
		20VII-L7SHX6	Feb. 6, 2009
The 4th leg of Chinese 49th Cruise (49 IV)	*Xiangyanghong 10*	49IV-L002SHX04	May 15, 2018
		49IV-L003SHX03	May 15–16, 2018
		49IV-L003SHX02	May 16–17, 2018
		49IV-L005SHX01	May 17–18, 2018
		49IV-L009SHX01c	May 25–26, 2018
		49IV-L010SHX02c	May 26–27, 2018

observed in the southwest corner of the Qiaoyue Seamount, implying that young volcanic activity may exist to the west. More than half of the collected samples are peridotites, suggesting that the basement is mostly exhumed mantle-derived plutonic. A small scarp (Fig. 2e) facing the Gallieni transform fault is visible and might be attributed to the stretching effect of the transform fault. The serpentinized peridotites and/or serpentine (Fig. 2f), as well as hydrothermally altered debris (Fig. 2g) were observed from cameras in certain areas.

4.2 *Potential hydrothermal activity*

The most distinct turbidity anomalies were observed on survey line 49IV-L003SHX02 on the Qiaoyue Seamount (Fig. 3a). The profile showed a concentrated plume layer at depths between –1 600 m and –2 000 m, with a maximum turbidity anomaly of 0.025 ΔNTU, similar to the result that detected nearby the high-temperature Perseverance vent field on the Mariana back-arc spreading center (Wang et al., 2021). Previous studies have shown that plume turbidity anomalies are almost induced by high-temperature venting (e.g., German et al., 2008; Baker et al., 2014, 2016; Son et al., 2014; Chen et al., 2019; Yue et al., 2019). Turbidity anomaly of 0.025 would be detected <10 km from the active vent (Chen et al., 2014; Tao et al., 2017; Wang et al., 2021). The horizontal scale of hydrothermal maximum was ~4 km (Fig. 3a) at the western crest of the Qiaoyue Seamount (Fig. 3b), indicating that active venting possibly occurs in the vicinity. Hydrothermal fluids discharge from vents usually ascending 300–500 m above the vent orifice until reaching the depth of neutral buoyancy (German et al., 2010; Schmale et al., 2012; Chen et al., 2014). In this study, the depths of the vent source would be –1 600 m to –2 500 m. The dispersal direction of hydrothermal plume is often affected by the regional bottom current. The overall westward bottom current in the study area indicates the active vent likely exists <10 km east of turbidity anomalies. As a result, we delineate the possible area of the hydrothermal vent on the northern flank of the Qiaoyue Seamount (Fig. 3b), consistent with the occurrence of suspected hydrothermally altered debris (Fig. 2g).

5 Discussion

5.1 *Morphotectonic analysis*

The SWIR is characterized by a series of linear seamounts that are approximately parallel to the ridge axis. These seamounts are usually viewed as resulting from magmatic supply and faulting (Mendel et al., 2003; Olive et al., 2015). Liu (2019) proposed that the presence of two detachment faults with opposite orientations on the flanks of the Qiaoyue Seamount, owing to the smooth seafloor and small dip angle (<10°) derived from the topography data (the resolution is ~100 m), as well as the exhumed mantle-derived rocks on the seafloor. This means that both flanks are the footwall of the two detachment faults. However, local higher resolution topography (a resolution of ~50 m) and video observations show different features. We recalculated the dip angle of both flanks and found that the value of the northern flank is ~9°, but the southern one is ~15°, which is larger than that reported by Liu (2019). There is no denying that there occur man-made measurement errors when estimating the angle of two flanks by calculating some across-seamount profile. The low-angle corrugated surface, with exposed exhumed mantle-derived peridotites on the northern flank of Qiaoyue Seamount, indicates that there exists a long-lived detachment fault with >12 km displacement. The corrugated surface is covered by thin sediments (Fig. 2a). Some block basalts were observed on the eastern crest of Qiaoyue Seamount which may stay in the early stage of the detachment process. Noticeably, although some peridotites were sampled, no gabbros were recovered on the corrugated surface. Due to relatively limited rock sampling, we could not preclude that gabbro exists at the subseafloor.

In contrast, the southern flank of Qiaoyue Seamount is characterized by a steeper and rougher surface (Supplementary Figs S1 and S2), which is unlikely to be detachment surface reported by Liu (2019). In addition, a large upper limit of south-facing fault scarp along the crest of the seamount was identified by high-resolution topography (Fig. 1 and Supplementary Figs S1 and S2), implying there likely exists a high-angle normal fault ~30 km in length. Therefore, we argued that the southern flank was more likely as the hanging wall of the high-angle normal fault, which was also supported by the occurrence of certain epicenters adjacent to the upper limit. This normal fault could lead to peridotites exposed (Fig. 2). Noticeable rock debris were observed at the crest of the Qiaoyue Seamount, which may also be linked with faulting.

Many authors have discussed the reason why a new high-angle fault initiates and cuts through the existing footwall of a detachment fault. Numerical modeling showed that when the magma supply is relatively poor, high-angle normal faults can form by breaking the footwall of the active master detachment fault (Tucholke et al., 2008). It is noteworthy that this model was run at a full spreading rate of 50 mm/a, roughly at the transition from slow to intermediate rates at MORs. Cannat et al. (2009) and Manatschal et al. (2011) found that the development of the steep fault may be a consequence of an increase in flexural rigidity and hence strengthening of the footwall. But this mechanism could not apply to ultra-slow spreading rate where the hydration of exhumed mantle will result in weakening of the footwall. The structure of the Qiaoyue Seamount is also seen at other regions of the ultra-slow spreading center (Cannat et al., 2006, 2019; Reston, 2018). Their formation mechanism has been studied by recent geodynamical modelling (Liu and Buck, 2018, 2020), they run model with full spreading rate of 15 mm/a and low magma supply and get the similar structure of the Qiaoyue Seamount.

It is worth noting that some studies suggest that numerous

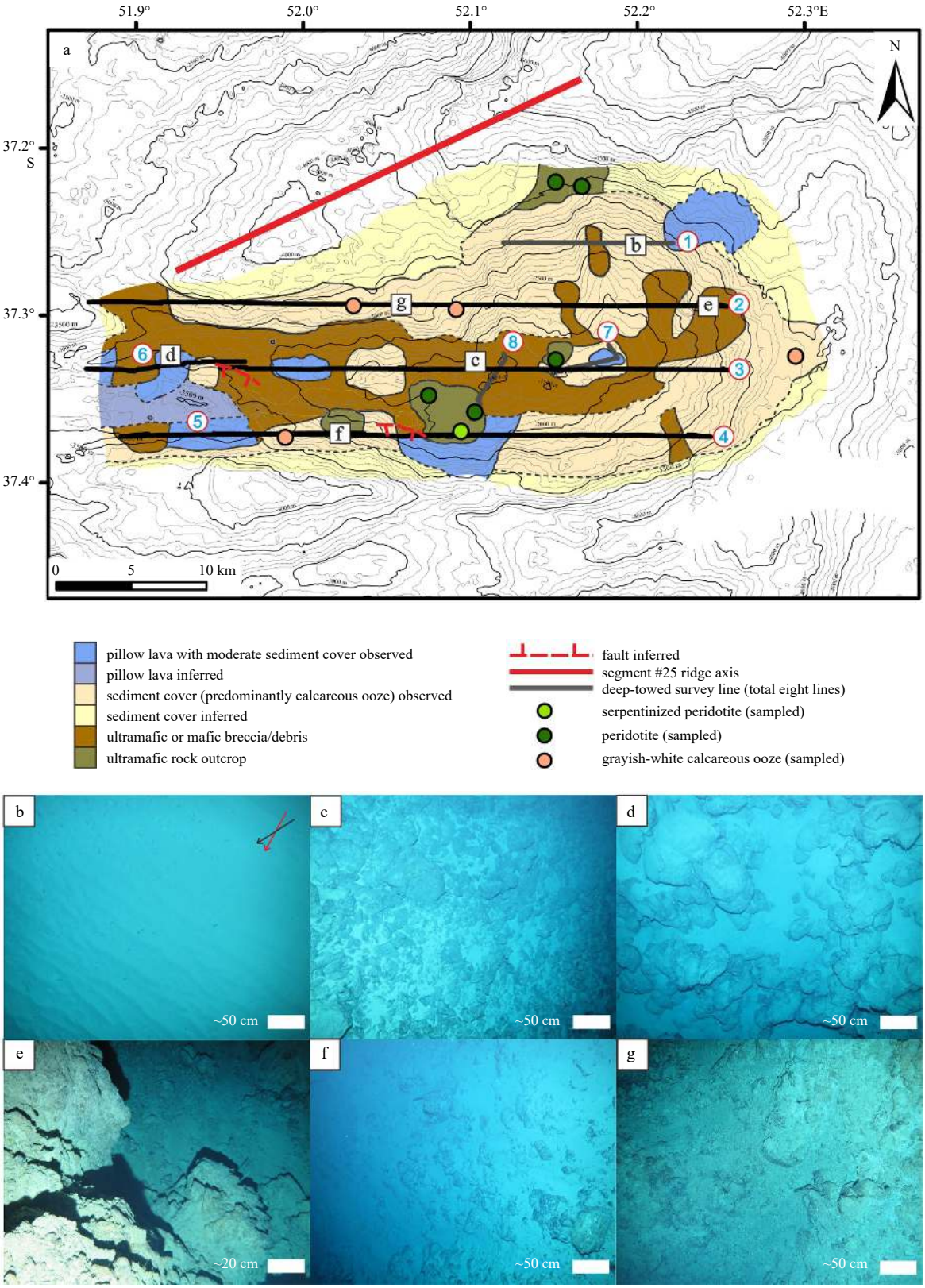

Fig. 2. Generalized geological map of the Qiaoyue Seamount, interpreted from the surface geology and locations of photographs features (a), pelagic sediment with ripple marks (the black and red arrows indicate the forward direction of the camera and the direction of the bottom currents, respectively) (b), rock breccia/debris covered with sediments (c), pillow lava covered with sediments (d), a small scarp with exposed rock/breccia (e), serpentinized peridotite and/or serpentine covered with thin-layer sediments (f), and suspected hydrothermally altered debris (g).

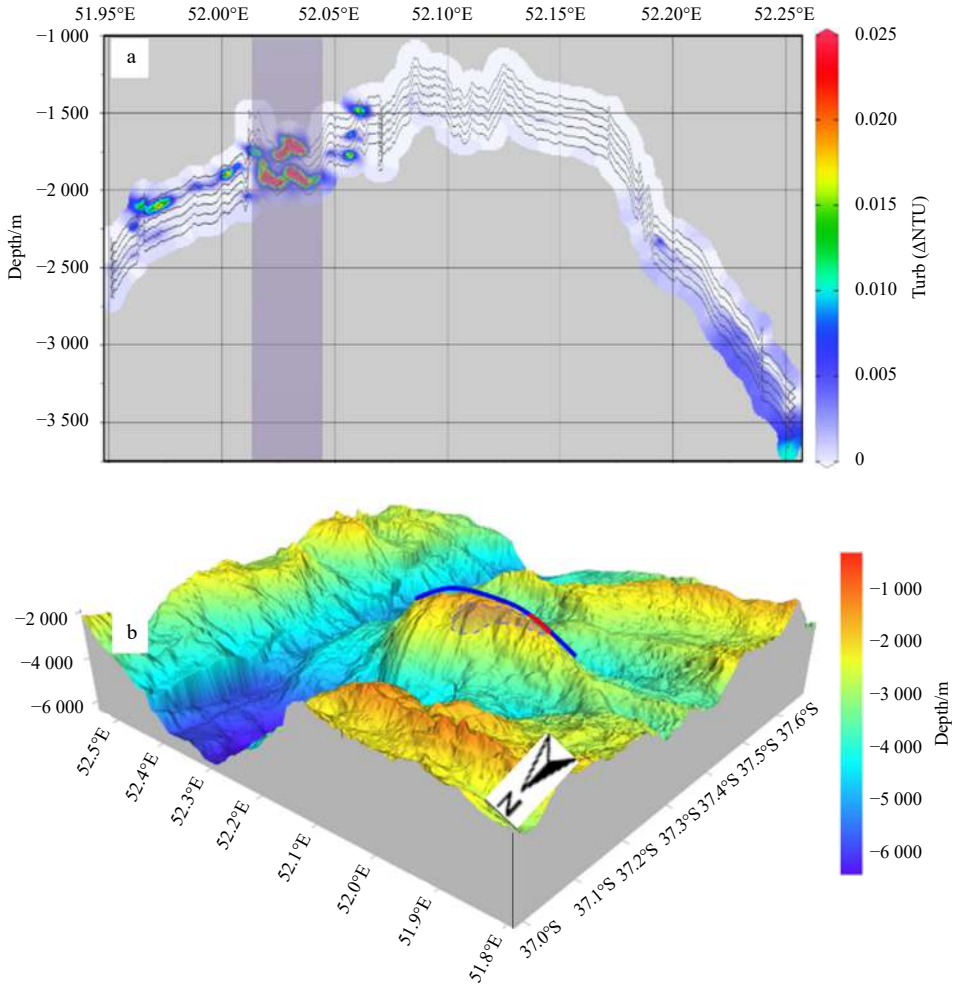

Fig. 3. Water column turbidity profile obtained from line ③ (in Fig. 2a) deep-towed survey line and the blue band show the range of the significant water column turbidity anomaly (0.02–0.025 ΔNTU) (a); blue translucent area indicates a potential hydrothermal venting field (the blue solid line shows line ③ survey line trace, while the red solid line indicates the trace of a significant water column turbidity anomaly) (b).

long-lived detachment faults with large-scale corrugations on magma-poor MORs may be associated with local elevated magmatism, especially on the later stage of detachment faulting (Cannat et al., 2006; Canales et al., 2008; MacLeod et al., 2009; Sauter et al., 2013). A new volcanic zone was located at the center of the spreading axis (Fig. 1), implying that there exists local enhanced magmatism even in magma-poor spreaing environment. In addition, small hummocky volcanic terrain was identified at the central crest of our study area, also supported by video observations. This may thus be linked with the local enhanced magmatism. However, fresh pillow lava (Fig. 2) were distributed in the southwest corner of Qiaoyue Seamount, which might be affected by the axial volcanic ridge of SWIR segment #26. Based on these results, we propose that a long-lived detachment fault exists at the northern flank and that the southern flank is the hanging wall of a new high-angle normal fault.

5.2 *Heat sources and fluid pathways*

The SWIR exhibits a limited magma supply and was considered to be lacking in hydrothermal activity (Baker et al., 2004). However, since the first active hydrothermal field (Longqi-1) was discovered on the SWIR in 2007, more hydrothermal fields have been observed in the area, including the Duanqiao-1, Yuhuang-1, Longqi-3, Junhui-1, Tiancheng-1, Tianzuo-1, and Changbai-1 fields (Tao et al., 2012, 2014). These discoveries indicate abundant hydrothermal activity along the SWIR. The potential hydrothermal activity associated with the detachment fault on the northern flank of Qiaoyue Seamount is possibly attributed to a high-temperature, ultramafic-hosted hydrothermal system (Fig. 4).

The occurrence of high-temperature hydrothermal activity at MORs requires sufficient heat sources and efficient hydrothermal circulation channels (Allen and Seyfried, 2004; Lowell, 2010). Lowell (2010) proposed that hydrothermal heat sources along the slow-spreading ridges were a combination of mantle upwelling, heat mining from the crust, exothermic chemical reactions, and magmatic heat sources. Local magma supply and crustal permeability have been proposed as the primary controllers of the distribution of hydrothermal activities along the SWIR (Tao et al., 2012). In addition, hydrothermal processes in ultramafic systems might be driven by regional heat flow, cooling gabbroic intrusions, and the heat of exothermic serpentinization reactions between seawater and mantle rocks (Fouquet et al., 2010). Noticeably, the exothermic heat cannot provide sufficient heat alone to drive a high-temperature hydrothermal system (Lowell, 2010). Furthmore, Lowell (2017) found that although ultramafic-

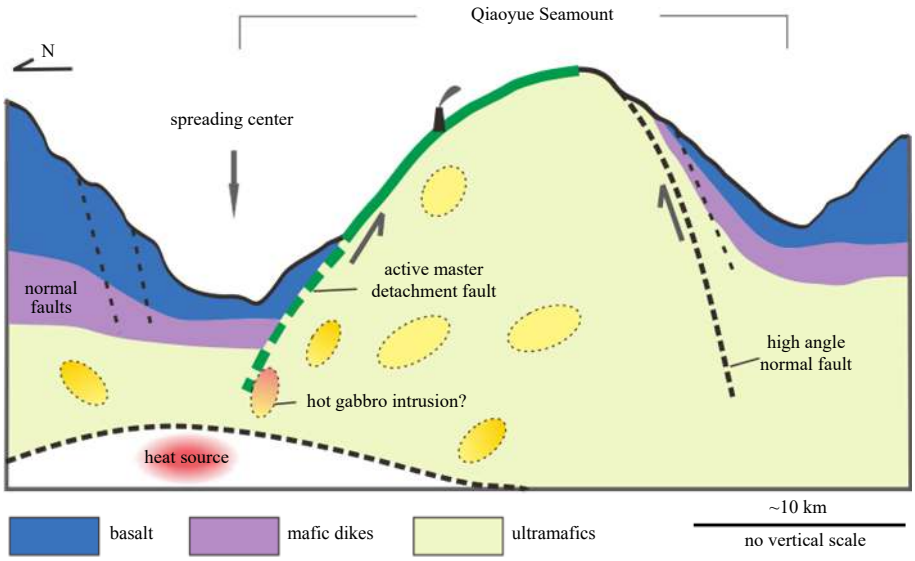

Fig. 4. Schematic model of hydrothermal system on the Qiaoyue Seamount.

hosted Lost City is a low-temperature (~91°C) hydrothermal system, it could only be driven by heat mined from the adjacent crustal but no need additional serpentinization of ultramafic rocks. A similar heat source was reported at the high-temperature off-axis Nibelungen hydrothermal vent (Melchert et al., 2008). Tao et al. (2020) suggested high-temperature Longqi-1 hydrothermal circulation was driven by a deep hot melt zone in the lithospheric mantle, which is associated with the deeply large-scale multi-stage detachment faulting system.

Compared to other high-temperature hydrothermal fields associated with detachment faults (Fouquet et al., 2010; Tao et al., 2020), the geological setting of the inferred high-temperature hydrothermal field on the Qiaoyue Seamount is similar to the Logatchev (Petersen et al., 2009) and Rainbow hydrothermal fields (Allen and Seyfried, 2004). Some plutonic or gabbroic intrusions in the footwall of detachment faults were proposed to be responsible for hydrothermal circulation at the Logatchev and Rainbow vents (Petersen et al., 2009; Pertsev et al., 2012; Sekhar and Lowell, 2015). Given the magmatic-tectonic process in our study area, the heat driving the inferred hydrothermal circulation would most likely be mined by a low-angle detachment fault from hot gabbroic intrusions in the footwall (Fig. 4).

The detachment fault could serve as the fluid pathway for hydrothermal circulation (Petersen et al., 2009). Fluid flow in seafloor hydrothermal systems is governed by subseafloor permeability and the nature of the heat sources (e.g., Wilcock and Fisher, 2004). Although some fields along the SWIR are located above an obvious heat source, as indicted by axial volcanic ridges, others are associated with fault systems (Tao et al., 2020) with higher focused permeability structure. The serpentinization of ultramafic rocks would induce a substantial volume expansion ranging between 25% and 45% for nearby rocks (Coleman, 1971). This volume expansion could promote cracking or faulting that would provide fluid access (Lowell, 2010) and high rock permeability. The high rock permeability associated with serpentinization along the detachment fault could foster efficient hydrothermal circulation channels (Fouquet et al., 2010; Dekov et al., 2018).

Overall, some hot gabbroic intrusions and high rock permeability are responsible for a high-temperature hydrothermal circulation situated at the footwall of the northern detachment fault of the Qiaoyue Seamount. In addition, more detailed surveys are needed to precisely locate the hydrothermal vent site and its heat source in the future.

6 Conclusions

In this study, our analyses reveal faults characteristics of Qiaoyue Seamount in relation to low magma supply. Through analyzing the observations from video and photos and water column turbidity anomalies, we predict a high-temperature, ultramafic-hosted hydrothermal system situated at the footwall of a northern detachment fault of the seamount. We propose that local gabbroic intrusions, coupled with high rock permeability lead to this hydrothermal circulation, even in a magma-poor spreading environment.

Acknowledgements

We are grateful to the captains and crews of the DY115-20 cruise on R/V *Dayang Yihao* and the DY135-49 cruise on R/V *Xiangyanghong 10*. We are also grateful to two anonymous reviewers for their constructive comments and suggestions.

References

Allen D E, Seyfried Jr W E. 2004. Serpentinization and heat generation: constraints from Lost City and Rainbow hydrothermal systems. Geochimica et Cosmochimica Acta, 68(6): 1347–1354, doi: 10.1016/j.gca.2003.09.003

Baker E T, Chen Y J, Morgan J P. 1996. The relationship between near-axis hydrothermal cooling and the spreading rate of mid-ocean ridges. Earth and Planetary Science Letters, 142(1–2): 137–145, doi: 10.1016/0012-821x(96)00097-0

Baker E T, Edmonds H N, Michael P J, et al. 2004. Hydrothermal venting in magma deserts: the ultraslow-spreading Gakkel and Southwest Indian Ridges. Geochemistry, Geophysics, Geosystems, 5(8): Q08002, doi: 10.1029/2004gc000712

Baker E T, German C R. 2004. On the global distribution of hydrothermal vent fields. In: German C R, Lin J, Parson L M, eds. Mid-Ocean Ridges: Hydrothermal Interactions Between the Lithosphere and Oceans. Washington, DC: American Geophysical Union, 245–266, doi: 10.1029/148gm10

Baker E T, Hémond C, Briais A, et al. 2014. Correlated patterns in hydrothermal plume distribution and apparent magmatic budget along 2500 km of the Southeast Indian Ridge. Geochemistry, Geophysics, Geosystems, 15(8): 3198–3211, doi: 10.1002/2014gc005344

Baker E T, Resing J A, Haymon R M, et al. 2016. How many vent fields? New estimates of vent field populations on ocean ridges from precise mapping of hydrothermal discharge locations. Earth and Planetary Science Letters, 449: 186–196, doi: 10.1016/j.epsl.2016.05.031

Beaulieu S E, Baker E T, German C R, et al. 2013. An authoritative global database for active submarine hydrothermal vent fields. Geochemistry, Geophysics, Geosystems, 14(11): 4892–4905, doi: 10.1002/2013gc004998

Beaulieu S E, Baker E T, German C R. 2015. Where are the undiscovered hydrothermal vents on oceanic spreading ridges?. Deep-Sea Research Part II: Topical Studies in Oceanography, 121: 202–212, doi: 10.1016/j.dsr2.2015.05.001

Buck W R, Lavier L L, Poliakov A N B. 2005. Modes of faulting at mid-ocean ridges. Nature, 434(7034): 719–723, doi: 10.1038/nature03358

Canales J P, Tucholke B E, Xu M, et al. 2008. Seismic evidence for large-scale compositional heterogeneity of oceanic core complexes. Geochemistry, Geophysics, Geosystems, 9(8): Q08002, doi: 10.1029/2008GC002009

Cannat M, Rommevaux-Jestin C, Sauter D. 1999. Formation of the axial relief at the very slow spreading Southwest Indian Ridge (49° to 69°E). Journal of Geophysical Research: Solid Earth, 104(B10): 22825–22843, doi: 10.1029/1999jb900195

Cannat M, Sauter D, Bezos A, et al. 2008. Spreading rate, spreading obliquity, and melt supply at the ultraslow spreading Southwest Indian Ridge. Geochemistry, Geophysics, Geosystems, 9(4): Q04002, doi: 10.1029/2007gc001676

Cannat M, Sauter D, Escartín J, et al. 2009. Oceanic corrugated surfaces and the strength of the axial lithosphere at slow spreading ridges. Earth and Planetary Science Letters, 288(1–2): 174–183, doi: 10.1016/j.epsl.2009.09.020

Cannat M, Sauter D, Lavier L, et al. 2019. On spreading modes and magma supply at slow and ultraslow mid-ocean ridges. Earth and Planetary Science Letters, 519: 223–233, doi: 10.1016/j.epsl.2019.05.012

Cannat M, Sauter D, Mendel V, et al. 2006. Modes of seafloor generation at a melt-poor ultraslow-spreading ridge. Geology, 34(7): 605–608, doi: 10.1130/g22486.1

Chen Jie, Tao Chunhui, Liang Jin, et al. 2018. Newly discovered hydrothermal fields along the ultraslow-spreading Southwest Indian Ridge around 63°E. Acta Oceanologica Sinica, 37(11): 61–67, doi: 10.1007/s13131-018-1333-y

Chen Sheng. 2016. The study of hydrothermal plume ore-prospecting criteria on the mid-ocean ridges (in Chinese)[dissertation]. Changchun: Jilin University

Chen Sheng, Tao Chunhui, Li Huaiming, et al. 2014. A data processing method for MAPR hydrothermal plume turbidity data and its application in the Precious Stone Mountain hydrothermal field. Acta Oceanologica Sinica, 33(8): 34–43, doi: 10.1007/s13131-014-0406-9

Chen Sheng, Tao Chunhui, Zhou Jianping, et al. 2019. The distribution characteristics of hydrothermal plume in mid-ocean ridge and its indicative role in polymetallic sulfide prospecting. Haiyang Xuebao (in Chinese), 41(8): 1–12, doi: 10.3969/j.issn.0253-4193.2019.08.002

Coleman R G. 1971. Petrologic and geophysical nature of serpentinites. Geological Society of America Bulletin, 82(4): 897–918, doi: 10.1130/0016-7606(1971)82[897:pagnos]2.0.co;2

Corliss J B, Dymond J, Gordon L I, et al. 1979. Submarine thermal springs on the Galápagos rift. Science, 203(4385): 1073–1083, doi: 10.1126/science.203.4385.1073

Dekov V M, Garbe-Schönberg D, Kamenov G D, et al. 2018. Redox changes in a seafloor hydrothermal system recorded in hematite-chalcopyrite chimneys. Chemical Geology, 483: 351–371, doi: 10.1016/j.chemgeo.2018.02.041

Dick H J B, Lin J, Schouten H. 2003. An ultraslow-spreading class of ocean ridge. Nature, 426(6965): 405–412, doi: 10.1038/nature02128

Dick H J B, Natland J H, Alt J C, et al. 2000. A long in situ section of the lower ocean crust: results of ODP Leg 176 drilling at the Southwest Indian Ridge. Earth and Planetary Science Letters, 179(1): 31–51, doi: 10.1016/s0012-821x(00)00102-3

Fouquet Y, Cambon P, Etoubleau J, et al. 2010. Geodiversity of hydrothermal processes along the Mid-Atlantic Ridge and ultramafic-hosted mineralization: a new type of oceanic Cu-Zn-Co-Au volcanogenic massive sulfide deposit. In: Rona P A, Devey C W, Dyment J, et al., eds. Diversity of Hydrothermal Systems on Slow Spreading Ocean Ridges. Washington, DC: American Geophysical Union, 321–367, doi: 10.1029/2008gm000746

Georgen J E, Lin J, Dick H J B. 2001. Evidence from gravity anomalies for interactions of the Marion and Bouvet hotspots with the Southwest Indian Ridge: effects of transform offsets. Earth and Planetary Science Letters, 187(3–4): 283–300, doi: 10.1016/s0012-821x(01)00293-x

German C R, Baker E T, Klinkhammer G. 1995. Regional setting of hydrothermal activity. Geological Society, London, Special Publications, 87(1): 3–15, doi: 10.1144/gsl.sp.1995.087.01.02

German C R, Baker E T, Mevel C, et al. 1998. Hydrothermal activity along the southwest Indian ridge. Nature, 395(6701): 490–493, doi: 10.1038/26730

German C R, Bowen A, Coleman M L, et al. 2010. Diverse styles of submarine venting on the ultraslow spreading Mid-Cayman Rise. Proceedings of the National Academy of Sciences of the United States of America, 107(32): 14020–14025, doi: 10.1073/pnas.1009205107

German C R, Petersen S, Hannington M D. 2016. Hydrothermal exploration of mid-ocean ridges: where might the largest sulfide deposits be forming?. Chemical Geology, 420: 114–126, doi: 10.1016/j.chemgeo.2015.11.006

German C R, Yoerger D R, Jakuba M, et al. 2008. Hydrothermal exploration with the Autonomous Benthic Explorer. Deep-Sea Research Part I: Oceanographic Research Papers, 55(2): 203–219, doi: 10.1016/j.dsr.2007.11.004

Han Xiqiu, Wu Guanghai, Cui R, et al. 2010. Discovery of a hydrothermal sulfide deposit on the Southwest Indian Ridge at 49.2°E. In: American Geophysical Union Fall Meeting 2010. San Francisco: AGU.

Hannington M, Jamieson J, Monecke T, et al. 2011. The abundance of seafloor massive sulfide deposits. Geology, 39(12): 1155–1158, doi: 10.1130/g32468.1

Hasenclever J, Theissen-Krah S, Rüpke L H, et al. 2014. Hybrid shallow on-axis and deep off-axis hydrothermal circulation at fast-spreading ridges. Nature, 508(7497): 508–512, doi: 10.1038/nature13174

Jian Hanchao, Singh S C, Chen Y J. 2017. Evidence of an axial magma chamber beneath the ultraslow-spreading Southwest Indian Ridge. Geology, 45(2): 143–146, doi: 10.1130/g38356.1

Kolla V, Bé A W H, Biscaye P E. 1976. Calcium carbonate distribution in the surface sediments of the Indian Ocean. Journal of Geophysical Research, 81(15): 2605–2616, doi: 10.1029/jc081i015p02605

Li Jiabiao, Jian Hanchao, Chen Y J, et al. 2015. Seismic observation of an extremely magmatic accretion at the ultraslow spreading Southwest Indian Ridge. Geophysical Research Letters, 42(8): 2656–2663, doi: 10.1002/2014gl062521

Li Huaiming, Tao Chunhui, Yue Xihe, et al. 2020. Enhanced hydrothermal activity on an ultraslow-spreading supersegment with a seismically detected melting anomaly. Marine Geology, 430: 106335, doi: 10.1016/j.margeo.2020.106335

Liu Chiheng. 2019. Tectono-magmatic characteristics of the Southwest Indian Ridge 46~52.5°E and its dynamic formation mechanism (in Chinese)[dissertation]. Beijing: Peking University

Liu Zhonglan, Buck W G. 2018. Magmatic controls on axial relief and faulting at mid-ocean ridges. Earth and Planetary Science Letters, 491: 226–237, doi: 10.1016/j.epsl.2018.03.045

Liu Zhonglan, Buck W R. 2020. Global trends of axial relief and faulting at plate spreading centers imply discrete magmatic events. Journal of Geophysical Research: Solid Earth, 125(8): e2020JB019465, doi: 10.1029/2020JB019465

Lowell R P. 2010. Hydrothermal circulation at slow spreading ridges: analysis of heat sources and heat transfer processes. In: Rona P A, Devey C W, Dyment J, et al., eds. Diversity of Hydrothermal Systems on Slow Spreading Ocean Ridges. Washington, DC: American Geophysical Union, 11–26, doi: 10.1029/2008gm000758

Lowell R P. 2017. A fault-driven circulation model for the Lost City Hydrothermal Field. Geophysical Research Letters, 44(6):

2703–2709, doi: 10.1002/2016GL072326
MacLeod C J, Searle R C, Murton B J, et al. 2009. Life cycle of oceanic core complexes. Earth and Planetary Science Letters, 287(3–4): 333–344, doi: 10.1016/j.epsl.2009.08.016
Manatschal G, Sauter D, Karpoff A M, et al. 2011. The chenaillet ophiolite in the French/Italian alps: an ancient analogue for an oceanic core complex?. Lithos, 124(3–4): 169–184, doi: 10.1016/j.lithos.2010.10.017
McCave I N, Kiefer T, Thornalley D J R, et al. 2005. Deep flow in the Madagascar-Mascarene Basin over the last 150000 years. Philosophical Transactions of the Royal Society A: Mathematical, Physical and Engineering Sciences, 363(1826): 81–99, doi: 10.1098/rsta.2004.1480
Melchert B, Devey C W, German C R, et al. 2008. First evidence for high-temperature off-axis venting of deep crustal/mantle heat: The Nibelungen hydrothermal field, southern Mid-Atlantic Ridge. Earth and Planetary Science Letters, 275(1–2): 61–69, doi: 10.1016/j.epsl.2008.08.010
Mendel V, Sauter D, Rommevaux-Jestin C, et al. 2003. Magmato-tectonic cyclicity at the ultra-slow spreading Southwest Indian Ridge: evidence from variations of axial volcanic ridge morphology and abyssal hills pattern. Geochemistry, Geophysics, Geosystems, 4(5): 9102, doi: 10.1029/2002gc000417
Muller M R, Minshull T A, White R S. 1999. Segmentation and melt supply at the Southwest Indian Ridge. Geology, 27(10): 867–870, doi: 10.1130/0091-7613(1999)027<0867:samsat>2.3.co;2
Olive J A, Behn M D, Ito G, et al. 2015. Sensitivity of seafloor bathymetry to climate-driven fluctuations in mid-ocean ridge magma supply. Science, 350(6258): 310–313, doi: 10.1126/science.aad0715
Pertsev A N, Bortnikov N S, Vlasov E A, et al. 2012. Recent massive sulfide deposits of the Semenov ore district, Mid-Atlantic Ridge, 13°31′ N: associated rocks of the oceanic core complex and their hydrothermal alteration. Geology of Ore Deposits, 54(5): 334–346, doi: 10.1134/s1075701512050030
Petersen S, Kuhn K, Kuhn T, et al. 2009. The geological setting of the ultramafic-hosted Logatchev hydrothermal field (14°45′N, Mid-Atlantic Ridge) and its influence on massive sulfide formation. Lithos, 112(1–2): 40–56, doi: 10.1016/j.lithos.2009.02.008
Reston T. 2018. Flipping detachments: the kinematics of ultraslow spreading ridges. Earth and Planetary Science Letters, 503: 144–157, doi: 10.1016/j.epsl.2018.09.032
Sauter D, Cannat M, Meyzen C, et al. 2009. Propagation of a melting anomaly along the ultraslow Southwest Indian Ridge between 46°E and 52°20′E: interaction with the Crozet hotspot?. Geophysical Journal International, 179(2): 687–699, doi: 10.1111/j.1365-246x.2009.04308.x
Sauter D, Cannat M, Rouméjon S, et al. 2013. Continuous exhumation of mantle-derived rocks at the Southwest Indian Ridge for 11 million years. Nature Geoscience, 6(4): 314–320, doi: 10.1038/ngeo1771
Sauter D, Patriat P, Rommevaux-Jestin C, et al. 2001. The Southwest Indian Ridge between 49°15′E and 57°E: focused accretion and magma redistribution. Earth and Planetary Science Letters, 192(3): 303–317, doi: 10.1016/s0012-821x(01)00455-1
Schmale O, Walter M, von Deimling J S, et al. 2012. Fluid and gas fluxes from the Logatchev hydrothermal vent area. Geochemistry, Geophysics, Geosystems, 13(7): Q07007, doi: 10.1029/2012gc004158
Sekhar P, Lowell R P. 2015. Numerical modeling of brine formation and serpentinization at the rainbow hydrothermal system. In: American Geophysical Union, Fall Meeting 2015. San Francisco: AGU
Son J, Pak S J, Kim J, et al. 2014. Tectonic and magmatic control of hydrothermal activity along the slow-spreading Central Indian Ridge, 8°S–17°S. Geochemistry, Geophysics, Geosystems, 15(5): 2011–2020, doi: 10.1002/2013GC005206
Tao Chunhui, Chen Sheng, Baker E T, et al. 2017. Hydrothermal plume mapping as a prospecting tool for seafloor sulfide deposits: a case study at the Zouyu-1 and Zouyu-2 hydrothermal fields in the southern Mid-Atlantic Ridge. Marine Geophysical Research, 38(1–2): 3–16, doi: 10.1007/s11001-016-9275-2
Tao Chunhui, Li Huaiming, Huang Wei, et al. 2011. Mineralogical and geochemical features of sulfide chimneys from the 49°39′E hydrothermal field on the Southwest Indian Ridge and their geological inferences. Chinese Science Bulletin, 56(26): 2828–2838, doi: 10.1007/s11434-011-4619-4
Tao Chunhui, Li Huaiming, Jin Xiaobing, et al. 2014. Seafloor hydrothermal activity and polymetallic sulfide exploration on the southwest Indian ridge. Chinese Science Bulletin, 59(19): 2266–2276, doi: 10.1007/s11434-014-0182-0
Tao Chunhui, Lin Jian, Guo Shiqin, et al. 2012. First active hydrothermal vents on an ultraslow-spreading center: southwest Indian Ridge. Geology, 40(1): 47–50, doi: 10.1130/G32389.1
Tao Chunhui, Seyfried Jr W E, Lowell R P, et al. 2020. Deep high-temperature hydrothermal circulation in a detachment faulting system on the ultra-slow spreading ridge. Nature Communications, 11(1): 1300, doi: 10.1038/s41467-020-15062-w
Tao Chunhui, Wu Guanghai, Ni Jun, et al. 2009. New hydrothermal fields found along the SWIR during the Legs 5-7 of the Chinese DY115-20 Expedition. In: American Geophysical Union Fall Meeting 2009. San Francisco: AGU
Tucholke B E, Behn M D, Buck W R, et al. 2008. Role of melt supply in oceanic detachment faulting and formation of megamullions. Geology, 36(6): 455–458, doi: 10.1130/g24639a.1
Wang Hu, Resing J A, Yan Qiaoyang, et al. 2021. The characteristics of Fe speciation and Fe-binding ligands in the Mariana back-arc hydrothermal plumes. Geochimica et Cosmochimica Acta, 292: 24–36, doi: 10.1016/j.gca.2020.09.016
Wilcock W S D, Fisher A T. 2004. Geophysical constraints on the subseafloor environment near mid-ocean ridges. In: Wilcock W S D, Delong E F, Kelley D S, et al., eds. The Subseafloor Biosphere at Mid-Ocean Ridges. Washington, DC: American Geophysical Union, 51–74, doi: 10.1029/144gm05
Yang Weifang, Tao Chunhui, Li Huaiming, et al. 2017. $^{230}Th/^{238}U$ dating of hydrothermal sulfides from Duanqiao hydrothermal field, Southwest Indian Ridge. Marine Geophysical Research, 38(1–2): 71–83, doi: 10.1007/s11001-016-9279-y
Yue Xihe, Li Huaiming, Ren Jianye, et al. 2019. Seafloor hydrothermal activity along mid-ocean ridge with strong melt supply: study from segment 27, southwest Indian ridge. Scientific Reports, 9(1): 9874, doi: 10.1038/s41598-019-46299-1
Zhou Huaiyang, Dick H J B. 2013. Thin crust as evidence for depleted mantle supporting the Marion Rise. Nature, 494(7436): 195–200, doi: 10.1038/nature11842

Supplementary information:

Fig. S1. Slope diagram of the Qiaoyue Seamount.

Fig. S2. Roughness diagram of the Qiaoyue Seamount.

Table S1. The observations for deep-towed surveys and sampling of the Qiaoyue Seamount.

The supplementary information is available online at https://doi.org/10.1007/s13131-021-1832-0 and www.aosocean.com. The supplementary information is published as submitted, without typesetting or editing. The responsibility for scientific accuracy and content remains entirely with the authors.